Development and characterization of a PLGA-HA composite material to fabricate 3D-printed scaffolds for bone tissue engineering

Joanna Babilotte, Benoit Martin, Vera Guduric, Reine Bareille, Rémy Agniel, Samantha Roques, Valérie Héroguez, Marc Dussauze, Manuel Gaudon, Damien Le Nihouannen, et al.

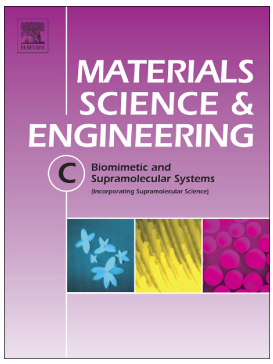

Development and Characterization of a PLGA-HA Composite Material to Fabricate 3D-printed Scaffolds for Bone Tissue Engineering

Joanna Babilotte, Benoit Martin, Vera Guduric, Reine Bareille, Rémy Agniel, Samantha Roques, Valérie Héroguez, Marc Dussauze, Manuel Gaudon, Damien Le Nihouannen, Sylvain Catros

PII: S0928-4931(20)33252-5

DOI: https://doi.org/10.1016/j.msec.2020.111334

Reference: MSC 111334

To appear in: *Materials Science & Engineering C*

Received date: 8 May 2020

Revised date: 30 July 2020

Accepted date: 2 August 2020

Please cite this article as: J. Babilotte, B. Martin, V. Guduric, et al., Development and Characterization of a PLGA-HA Composite Material to Fabricate 3D-printed Scaffolds for Bone Tissue Engineering, *Materials Science & Engineering C* (2020), https://doi.org/10.1016/j.msec.2020.111334

Development and Characterization of a PLGA-HA Composite Material to Fabricate 3D-printed Scaffolds for Bone Tissue Engineering

Joanna Babilotte[1], Benoit Martin[1], Vera Guduric[1], Reine Bareille[1], Rémy Agniel[2], Samantha Roques[3], Valérie Héroguez[4], Marc Dussauze[5], Manuel Gaudon[6], Damien Le Nihouannen[1], Sylvain Catros[7*]
[1]Univ. Bordeaux, INSERM, BioTis U1026, 33076 Bordeaux, France
[2]CY Cergy Paris Université, Maison Internationale de la Recherche, Lab. ERRMECe, 95031 Neuville-Oise, France
[3]Univ. Bordeaux, CIC1401, CHU Bordeaux, Inserm, 33076 Bordeaux, France
[4]Laboratoire de Chimie des Polymères Organiques, CNRS, Bordeaux INP, UMR5629, 33607 Pessac, France
[5]Univ. Bordeaux, Institut des Sciences Moléculaires, UMR 5255 CNRS, 33405 Talence, France
[6]CNRS, Univ. Bordeaux, Bordeaux INP, ICMCB, UMR5026, 33608 Pessac, France
[7]Univ. Bordeaux, INSERM, BioTis U1026, CHU Bordeaux, Dentistry and Oral Health Department, 33076 Bordeaux, France
*Corresponding author
Université de Bordeaux, INSERM, BioTis U1026, 146 rue Léo Saignat, 33076 Bordeaux, France
Email: sylvain.catros@inserm.fr

Abstract

Additive manufacturing is a rising field in bone tissue engineering. Additive fabrication offers reproducibility, high precision and rapid manufacture of custom patient-specific scaffolds. The development of appropriate composite materials for biomedical applications is critical to reach clinical application of these novel biomaterials. In this work, medical grade poly(lactic-co-glycolic) acid (PLGA) was mixed with hydroxyapatite nanoparticles (nHA) to fabricate 3D porous scaffolds by Fused Deposition Modeling. We have first confirmed that the composite material could be printed in a reproductive manner. Physical characterization demonstrated a low degradation of the material during manufacturing steps and an expected loading and homogeneous distribution of nHA. *In vitro* biodegradation of the scaffolds showed modifications of morphological and physicochemical properties over time. The composite scaffolds were biocompatible and high cell viability was observed *in vitro*, as well as a maintain of cell proliferation. As expected, the addition of nHA displayed a positive impact on osteodifferentiation *in vitro*. Furthermore, a limited inflammatory reaction was observed after subcutaneous implantation of the materials in the rat. Overall, this study suggests that this composite material is suitable for bone tissue engineering applications.

Keywords: Fused Deposition Modeling, Bone Tissue Engineering, Composite, Polymer, Hydroxyapatite

1. Introduction

Oral and maxillofacial bone loss can occur in the cases of trauma, infection or tumor removal. Even if autologous bone can be used in several clinical situations, it shows some drawbacks due to the induced

donor site morbidity and limited bone availability. A variety of natural and synthetic biomaterials have been developed to promote bone regeneration as alternatives to autologous bone grafts [1,2]. Biomaterials are expected to restore function and esthetics, especially in the case of dental implant rehabilitations [2]. The ideal biomaterial should be biocompatible, bioresorbable, osteoconductive and if possible osteoinductive and osteogenic. It means that it should provide a cell-friendly structure and be resorbed in order to leave space for the newly-formed bone.

One of major limitations of current bone materials used in clinics is the difficulty to produce complex anatomical shapes, which leads to poor adaptation to the defect margins, especially in the oral and maxillofacial area. A long and complex procedure might be needed to shape biomaterials during surgery, which inherently extends surgical time, and may eventually increase the risk of post-operative complications [3]. Additive manufacturing technologies have garnered enormous attention, thus offering a new and promising approach for bone repair and regeneration. Indeed, they offer the possibility to fabricate precise complex microporous architecture, with reproducible size, shape and interconnectivity of pores to mimic the natural microarchitecture of bone. Moreover, these technologies are used to fabricate custom-made scaffolds that meet the specific clinical needs of patients with bone defects [4,5].

Several fabrication technologies have been applied in regenerative medicine to process scaffolds with a defined architecture. According to Moroni et al. , the current additive manufacturing methods can be described as “Light-based” technologies (selective laser sintering, stereolithography, two-photon polymerization), 3D printing, fused deposition modeling, ink-jet printing, 3D plotting, and solution and melt electrospinning [6]. In this study, we used Fused Deposition Modeling (FDM) to fabricate composite scaffolds. FDM is a common technique for scaffold fabrication based on material extrusion: a heated extrusion head forces out a thermoplastic filament material and deposits the semi-molten polymer onto a platform, heated or not, in a layer-by-layer process. FDM enables the fabrication of controlled and regular structure scaffolds with good structural integrity and mechanical properties, due to a fusion between material layers [7,8].

A wide range of materials show interesting properties for the development of bone scaffolds: mostly natural or synthetic polymers and ceramics [9]. However, due to the technical specifications of 3D printers, all of the conventional bone biomaterials cannot be printed in their original composition. For example, Fused

Deposition Modeling printers require thermoplastic biomaterials in the shape of filament with specific diameter [6].

Biocompatible and biodegradable polymers are commonly used for tissue engineering scaffolding. Numerous degradable polymers such as polycaprolactone (PCL), polylactic acid (PLA), poly(lactic-co-glycolic) acid (PLGA), are compatible with FDM technology. They offer a good support for cell attachment, anchorage and proliferation [10]. However, they are usually not sufficient to assure a complete bone reparation due to their lack of osteo-promotive ability [10,11].

For bone tissue regeneration, mineral-based materials play a major role. Hydroxyapatite (HA) and β-tricalcium phosphate (β-TCP) are the most extensively studied minerals for bone scaffolds [12]. They are frequently used because of their similarities in structure and composition with the inorganic elements of human bone. Their compressive strength [13–16] and potential for osteoconductivity [17] make them the materials of choice for bone tissue engineering strategies. However, these calcium phosphates could be difficult to print and they might require a post-printing step [1,11].

The development of 3D-printed scaffolds for bone regeneration includes to go beyond the limitations related to each type of material. Hence, it was proposed to develop combinations of biomaterials to obtain composite materials. Recent literature reviews reported that the combination of a synthetic polymer material with a ceramic material could be used to counterbalance their respective limitations [10,12]. It was reported that such composite scaffolds displayed increased osseointegration and bone formation, compared to raw biomaterials [10,12].

The aim of this work was to synthesize and characterize a composite biomaterial made of medical grade poly(lactic-co-glycolic) acid (PLGA) mixed with 5% or 10% (w/w) hydroxyapatite nanoparticles (nHA): this biomaterial was designed to fabricate 3D-printed scaffolds for bone tissue engineering. Initially, the printing quality obtained with PLGA, PLGA-HA 5% and PLGA-HA 10%, was evaluated. Then the materials were characterized using various physical characterization techniques. The chemical degradation of the polymer during the different fabrication steps was evaluated, the real mineral charge was verified, the type of nHA was identified and nHA distribution was observed. Further, *in vitro* biodegradation of the scaffolds was evaluated: morphological and physicochemical properties modifications were observed. Then the biocompatibility was tested *in vitro* and *in vivo*. Two cell types were used *in vitro*: human bone marrow

stromal cells (hBMSCs) and human adipose-derived stem cells (hADSCs). Preliminary assays to evaluate cell differentiation were performed to validate potential applications of this composite material for future bone grafts applications.

2. Material and methods

2.1. Fabrication and design of PLGA-HA materials

Nano-hydroxyapatite (nHA) was prepared by wet chemical precipitation as described by Afshar et al. [18] at room temperature by the addition of an orthophosphoric acid solution (H_3PO_4) into a calcium hydroxide solution ($Ca(OH)_2$). Solid pellets of PLGA (PURASORB® PLG 8218, Corbion) were mixed with different filler percentage of nHA powder. The filler content was 5% or 10% wt of nHA. The different mix were melted at 195°C and extruded into a filament of 1.75 mm diameter using a twin-screw extruder (Pharma 11 HME Thermofisher).

Rhino 6® and Clump generator software® were used to design porous 400 µm thick scaffolds with 350*350µm (0.122 mm^2) squared pores and threads of 200 µm width. Scaffolds were manufactured using a custom-made 3D FDM printer (MicroPrint, IUT de Bordeaux, France) with a nozzle of 400 µm [19]. The printing temperature was set to 165-170°C, 170-175°C and 175-180°C to print respectively PLGA-HA 10%, PLGA-HA 5% and PLGA. Prior to evaluations, printed scaffolds were sterilized by gamma irradiation (25 kGy, room temperature; Nordion®, GC 5000).

PLGA, PLGA-HA 5% and PLGA-HA 10% porous scaffolds were printed, then the macro- and micro-structure of scaffolds were observed using binocular (Leica®, MZ10F) and scanning electron microscope (GeminiSEM300, Zeiss). To confirm the reliability of the printing technique, expected pore size was compared with the actual pore dimensions of printed scaffolds. For each material, six scaffolds were printed and images were taken using binocular microscopy. After thresholding the images with ImageJ® software (NIH), DiameterJ® plug-in was used to automatically calculate pores dimensions.

2.2. Physicochemical analysis of scaffolds

To evaluate chemical degradation during manufacturing steps and *in vitro* degradation, the average molecular weight ($\overline{M}_w$) and polydispersity index (PDI) of PLGA in composites was determined by Size

Exclusion Chromatography (SEC) using tetrahydrofuran (THF) as the eluent. The samples of PLGA, PLGA-HA 5% and PLGA-HA 10% were dissolved in THF on a shaker for 1 day and filtered with a 0.45 µm polyamide membrane. Measurements in THF were performed on an Ultimate 3000 system (Thermoscientific) equipped with a diode array detector. The system also included a multi-angles light scattering detector and a differential refractive index detector (Wyatt technology). Polymers were separated on three G2000, G3000 and G4000 TOSOH HXL gel columns (300 x 7.8 mm, exclusion limits from 1000 Da to 400 000 Da) at a flowrate of 1 mL/min. Columns temperature was held at 40°C. Easivial kit® of polystyrene from Agilent was used as standard.

The thermal degradation of the polymer and the mineral content (nHA) within the scaffolds were assessed by thermogravimetric analysis, using a TA instrument TG50. The analysis was performed according to MO093 and ISO 11358 norms. The analysis was carried out on PLGA pellets (raw material) and materials before and after FDM printing. The samples were warmed from 25°C to 900°C (sequential increase of 10°C/min) then an isotherm was performed during 60 min at 900°C.

Structural properties were explored by X-ray diffraction (XRD) using a diffractometer (Bragg Brentano Theta-Theta geometry), with a copper anticathode (CuKα, λ = 0.154 nm) source. The working tension and intensity were 40 kV and 40 mA, respectively, with collection of a spectrum on 2Θ = 10°–60° range and a step of 0.017°.

The mechanical properties were investigated with a uniaxial tensile test using an Autograph AGS-X (Shimadzu®). Tests were conducted on porous material described before at 10 mm/min until failure to evaluate tensile strength.

2.3. Nano-Hydroxyapatite distribution

The molecular constituents of the composite material and the nHA distribution in the materials were evaluated by Raman spectroscopy (Xplora, Horiba Scientific). Briefly, a 532 nm laser was used for excitation and spectra of printed and non-printed of PLGA with nHA were recorded. Spectra of the pure nHA, as well as printed and non-printed PLGA were recorded as controls. Phosphate peak (960 cm^{-1}), specific for nHA, was used on samples for cartography of nHA distribution.

nHA spatial distribution in the materials was evaluated with X-ray microtomography (SkyScan 1276 micro-CT system, Bruker). The X-ray source was set at 50 kV and 120 µA. Samples of PLGA-HA 5% and PLGA-HA 10% before (filaments) and after printing (scaffolds) were imaged with a 3D isotropic voxel size of 8 µm. The 3D reconstructions were performed using CT Analyzer v. 1.17.7.2 + software.

2.4. *In vitro* degradation of the materials

The *in vitro* degradation of materials was performed according to the norm ASTM-F1635. Porous scaffolds of PLGA and PLGA-HA 10% were immersed in PBS (DPBS 1X, without Ca and Mg) and incubated at 37°C in a 5% CO_2 incubator for 15 weeks. Each week, pH was measured with a pHmeter (Fisher Scientific accumet® AE150 with PerpHecT® ROSS® Micro pH Electrode). The PBS solution was changed and collected every week during degradation. At different time points (2, 4, 6, 8, 10, 11, 12, 13, 14, 15 weeks), the scaffolds were weighed and day 0 was defined as the baseline. The chemical degradation was evaluated by SEC at week 0, 2, 6, 10, 12, 15 using the protocol described above. The Ca^{2+} release during degradation was measured in the PBS collected, using a fluorometric assay kit (Calcium Quantification Kit (ab11215). Finally, the scaffolds were observed by Scanning Electron Microscopy (Zeiss GeminiSEM300) after Ni coating, to evaluate the surface structural changes at weeks 0, 6 and 15.

2.5. Cell culture and cell seeding

All human samples were collected in accordance with the French Ministry of Higher Education and Research and National Institute for Health and Medical Research (agreement DC-2008–412). Human adipose-derived stem cells (hADSCs) were isolated from subcutaneous fatty tissue from human skin biopsies during plastic surgeries [20]. Fatty tissue was separated from the skin and minced with a scalpel. Afterwards, the fatty tissue was digested with type I collagenase (Worthington, CLSO1, 1mg/mL in PBS 1X BSA 2%) for 1h30 at 37°C under agitation (250 rpm). After centrifugation, the pellet was resuspended in ELB buffer (NH_4Cl 155 mM, K_2HPO_4 5.7 mM, EDTA 0.1 mM, pH 7.3) and sequentially filtered through a 100 µM, 70 µM, 40 µM nylon cell strainer (BD Falcon™). The filtrate was centrifuged and the pellet was resuspended in DMEM/F-12 GlutaMAX (Gibco®, Cat No.31331-028) supplemented with 10% Fetal Bovine Serum (FBS; Biowest®) and 0.1% antibiotics (Pen Strep, Gibco®). Human bone marrow stromal cells (hBMSCs) were isolated from bone marrow samples, which were collected during orthopedic surgeries according to Vilamitjana-Amédée et al. [21], with some modifications [22]. Briefly, a single-cell suspension was obtained

by sequential passages of aspiration through 16-, 18-, and then 21-gauge needles. After centrifugation the pellet was resuspended in Alpha-MEM (Gibco®, Cat No. A10400-02), supplemented with 10% FBS and 0.1% antibiotics (Pen Strep, Gibco®).

Cells from mixed donors at early passages (3 or 4) were used for the different experiments. Cell culture on porous scaffolds were performed in 24-well plates. Each well was coated with agarose (2% (w/v) in 1X PBS; Sigma-Aldrich Co, A9539) before adding scaffolds, to avoid cell adhesion on the tissue culture plastic. Cells were seeded at a density of 75 000 cells/cm^2 on materials and 5 000 cells/cm^2 on plastic wells and incubated at 37°C in a humidified atmosphere containing 5% CO_2 in air.

2.6. *In vitro* biocompatibility

The cytotoxicity of potential release compounds was evaluated, according to the norm NF EN 30993-5 ISO 10993-5. Cell viability was evaluated by neutral red and metabolic activity was evaluated by MTT. Neutral red assay is based on the accumulation of neutral red dye in the lysosomes of viable cells. The MTT assay is based on the activity of NADPH-dependent cellular oxidoreductase enzymes. For both assays, medium extracts were prepared by incubating scaffolds in cell culture media with a specific ratio between the immersed surface of the scaffold and the volume of the medium (from 3 to 6 cm^2/mL). Five scaffolds of each material were incubated in appropriate cell medium for 3 days at 37°C in a humidified atmosphere containing 5% CO_2 in air. Medium extracts were collected after 1 (E1), 2 (E2), and 3 days (E3) and stored at 4°C. For both assays, hADSCs and hBMSC were plated at 15 000 cells/cm^2 in 96-well plates and cultured during 72 h to reach subconfluence (80%). After removal of culture media, medium extracts (E1, E2, and E3) supplemented with 10% FBS (v/v) were added. Triton 100X (0.1%) was used as positive control and cell culture medium alone was used as negative control (5 wells for each condition). Plates were incubated at 37°C in a 5% CO_2 incubator for 24h. The MTT stock solution (5 mg/mL in 0.1M PBS, pH = 7.4; Sigma-Aldrich, Cat No M2128) was diluted (20% in IMDM without phenol red, Gibco®, Cat No. 21056-023) and this solution was added in each well. After 3h of incubation at 37°C in a humidified atmosphere containing 5% CO_2 in air, the solution was removed, and formed formazan crystals were dissolved by adding dimethyl sulfoxide (DMSO; Sigma-Aldrich, Cat No. D5879-1L). Staining intensity was quantified by measuring the absorbance at 540 nm using a spectrophotometer (Perkin Elmer®, 2030 Multilabel Reader Victor™ X3). The Neutral Red (Sigma-Aldrich, N4638) was diluted (1.25% w/v) in IMDM supplemented with 10% FBS)

and this solution was added in each well. After 3h of incubation at 37°C in a humidified atmosphere containing 5% CO_2 in air, the solution was removed, and cells were lysed with a solution made of 1% acetic acid in 50% ethanol. Staining intensity was quantified by measuring the absorbance at 540 nm using a spectrophotometer (Perkin Elmer®, 2030 Multilabel Reader Victor™ X3).

Cell viability was also tested by Live-Dead staining (Invitrogen®, Cat No L3224), which was based on acetoxymethylester of calcein (Calcein-AM) and ethidium homodimer-1 (EthD-1). Calcein-AM is cleaved in the cytoplasm by esterase and thus indicated live cells showing a green fluorescence. EthD-1 enters cells with damaged membranes and binds to nucleic acids, producing a red fluorescence of dead cells. Both cells types were seeded on PLGA and PLGA-HA 10% porous scaffolds as described before. After 7, 14 and 21 days of culture, the samples were incubated with the solution of Calcein-AM and EthD-1. After incubating for 15 min in the dark in a humidified atmosphere with 5% CO_2 at 37 °C., images were acquired using a confocal laser scanning microscope (Leica, TSC SPE DM 4000B).

2.7. *In vitro* cell differentiation

To assess the osteogenic capacity of hADSCs an hBMSCs seeded on the different scaffolds, the Alkaline Phosphatase (ALP) activity was evaluated through semiquantitative staining. ALP kit (Sigma, 85L3R) was used following the manufacturer's instructions. At designated time-points (3, 7 and 14 days), the cells were fixed for 30 sec in citrate (15 mM) acetone mix (2:3 v/v) and the samples were incubated for 30 min with ALP stain. After staining, images of the scaffolds were taken with a binocular microscope (Leica®, MZ10F).

Secondly, the synthesis of mineralized matrix was evaluated by Red Alizarin staining. On day 21, cells were washed three times with PBS, fixed in PFA 4% for 10 min, washed twice with distilled deionized (DD) water, and stained with Alizarin Red solution (2%, pH 4.2) for 10 min at room temperature. Then, they were washed several times with DD water to remove excess stain. Finally, images of the samples were taken using binocular microscope (Leica®, MZ10F). Quantification of the staining was performed by extraction with cetylpyridinium chloride solution (100 mM). The supernatant was collected for absorbance measurements at 570 nm (Victor X3 2030 Perkin Elmer).

2.8. *In vivo* biocompatibility

The present study was approved by the French Ethics Committee (agreement APAFIS n° 4375-2016030408537165v8). The biocompatibility of PLGA and PLGA-HA 10% were assessed using a rat subcutaneous implant model. Sixteen 8 weeks old male Wistar rats were used. Surgery was carried out under aseptic conditions. Short-term anesthesia was induced by inhalation of 4% isoflurane (air:1.5 L/min) and maintained using isoflurane 2% (air: 0.4 L/min). Analgesia was performed by intraperitoneal injection of 0.1 mg/kg buprenorphine (Buprecare®, 0.3 mg/mL). The back of rats was shaved, the surgical site was aseptically prepared, and a midsagittal incision was made in the back area. Two conditions were implanted on both sides of the mid-dorsal line (4 materials per rat). In addition, a sham-operated control with no biomaterial implantation was performed for this study. After surgery, food and water were supplied ad libitum. Euthanasia was performed one week and 4 weeks after implantation using CO_2 inhalation (n=16 rats; 8 rats per time point). After shaving, the samples were carefully harvested and rinsed with PBS 1x, then placed in 4% paraformaldehyde (Antigenfix, Microm Microtech, France) overnight. Then, the explanted samples were rinsed in PBS 1x and processed for histology. Samples were dehydrated and processed for conventional embedding in paraffin. Ten-µm-thick serial sections were made. Sections were stained with hematoxylin-eosin-safran (HES). Images were acquired with a slide scanner (Hamamatsu Nanozoomer 2.0HT). According to the NF-EN-ISO 10993-6 standard, a blinded independent trained investigator scored the inflammatory reaction around the implants semi-quantitatively. The following biological response parameters were assessed and recorded: cellular infiltration and inflammatory cell type (polymorphonuclear, lymphocytes, macrophages, plasma cells and giant cells), vascularization, fatty infiltration and extent of fibrosis. The scoring system was as follows: the test sample was considered as non-irritant (N: 0.0 up to 2.9), slightly irritant (S: 3.0 up to 8.9), moderately irritant (M: 9.0 up to 15.0) or severely irritant (I > 15) to the tissue as compared to the sham-operated control sample.

2.9. Statistical analysis

The results were expressed as mean ± standard deviation, with n indicating the number of samples tested per conditions. Statistical analysis was performed using GraphPad Prism® Software (La Jolla/CA, USA). First, a normality test was performed using a D'Agostino and Pearson omnibus normality test. If data assumed Gaussian distribution, differences were assessed by one-way analysis of variance (ANOVA) with the Bonferroni post-test, whereas statistical significance for independent samples was evaluated with the

non-parametric Kruskal-Wallis test followed by Dunn's multiple comparison test. In both cases, statistical significances are marked by stars with * indicating a two-tailed $p < 0.05$, ** $p < 0.01$, and *** $p < 0.001$.

3. Results

3.1. Fabrication and design of PLGA-HA materials

All scaffolds (PLGA, PLGA-HA 5% and PLGA-HA 10%) were printed in the shape of a mesh with square pores, inside a solid frame (Fig. 1.A). These three different composite materials were used for the physicochemical evaluation. After this first part, 2 materials (PLGA and PLGA-HA 10%) were selected for *in vitro* and *in vivo* tests.

First, we observed that the addition of nHA particles decreased the printing temperature of materials. PLGA was printed at 175-180°C whereas PLGA-HA 5% and PLGA-HA 10% were printed at 170-175°C and 165-170°C respectively. Macroscopic and microscopic observations using binocular (Fig. 1.A) and scanning electron microscopy (SEM, Fig. 1.B) of the scaffolds showed regular straight threads printed layer-by-layer in both horizontal and vertical directions with perpendicular crossings. SEM was used to evaluate the surface features of the porous scaffolds (Fig. 1.B.): PLGA scaffolds displayed a smooth surface, while PLGA-HA scaffolds surface displayed a rough and irregular appearance. This irregular surface corresponded to the loaded materials and was most likely nHA particles, as they were more numerous with increasing nHA concentration. PLGA thread appeared thinner (Fig. 1.A/B) and to study whether the printing technology was precise and reproducible, we quantified the pore size of printed scaffolds (Fig. 1.C). Image analysis showed that pore sizes of PLGA scaffolds were statistically higher than the predicted value (0.122 mm^2) by 13 ± 8 % (0.137 ± 0.013 mm^2). Pore sizes of PLGA-HA 5% scaffolds were statistically lower by 18 ± 6 % (0.100 ± 0.007 mm^2). PLGA-HA 10% scaffolds showed the highest reliability with pore size 99 ± 5 % (0.122 ± 0.006 mm^2) of the predicted value. Thus, while the printing process was reproducible (with SDs < 10% of measured values), printed scaffolds exhibited expected pore size dimension only for PLGA-HA 10% scaffolds (Fig. 1.C).

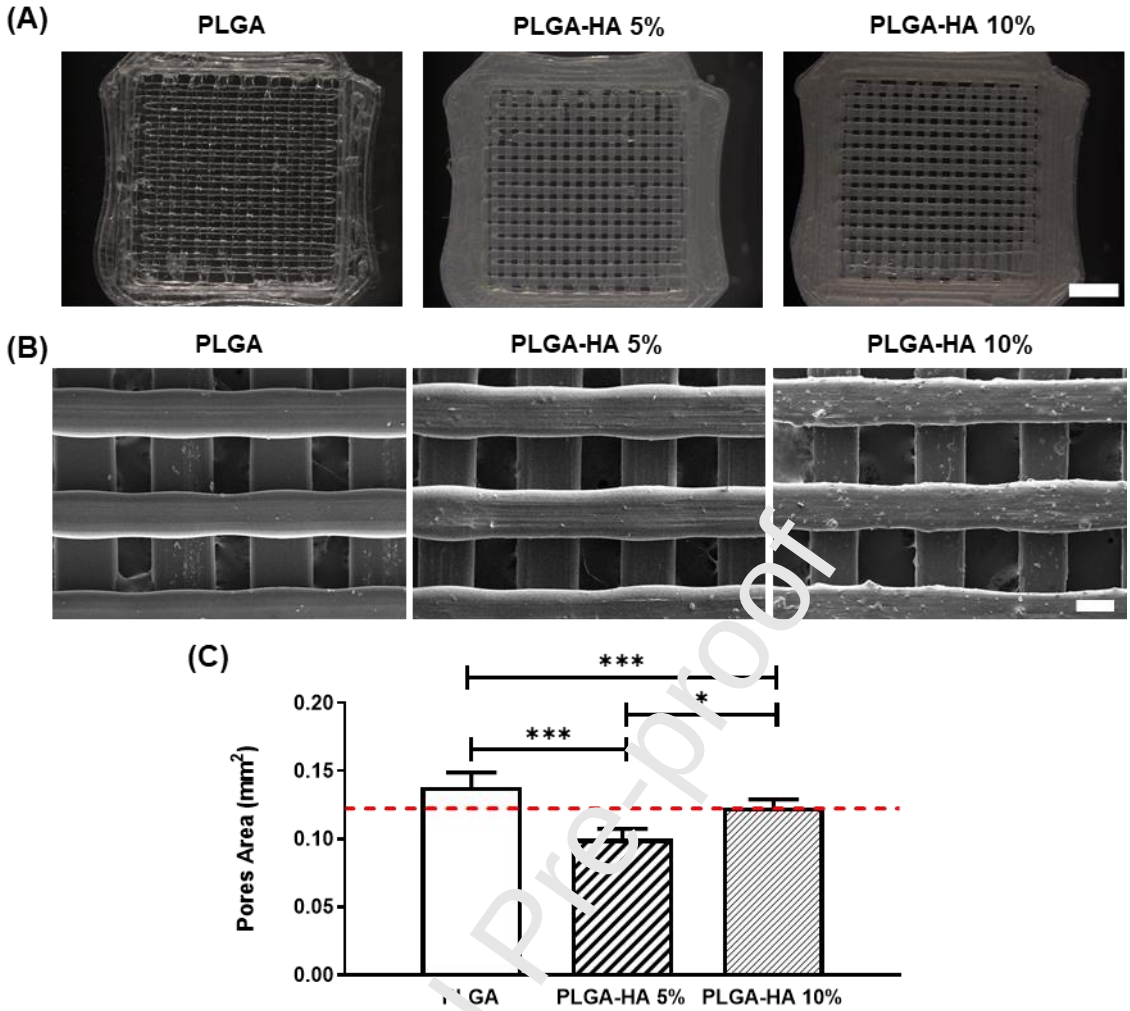

Figure 1. Morphological evaluation of printed scaffolds. Scaffolds of PLGA, PLGA-HA 5% and PLGA-HA 10% were imaged using binocular microscope (Scale bar = 2 mm) **(A)** and scanning electron microscope (Scale bar = 200 µm) **(B)**. Printing accuracy was analyzed by quantification of pore sizes on printed scaffolds. DiameterJ plug-in was used to calculate pore dimensions on pictures acquired by binocular microscope. Dotted red line indicates the predicted value. Data are mean ± SD (n=6, * $p<0.05$, ** $p < 0.01$, and *** $p < 0.001$) **(C)**.

3.2. Physicochemical analysis of scaffolds

SEC was used to determine the effect of filament shaping and 3D printing by FDM on the average molecular weight ($\bar{M}_w$) and polydispersity index (PDI) of PLGA (Fig. 2.A). SEC has shown a reduced variation

(A)

	PLGA		PLGA-HA 5%		PLGA-HA 10%	
	$\bar{M}_w$ (g/mol)	PDI	$\bar{M}_w$ (g/mol)	PDI	$\bar{M}_w$ (g/mol)	PDI
Raw	244 104	2.4	/	/	/	/
Before printing	221 799	2.6	158 586	2.5	169 348	2.4
After printing	221 144	2.0	149 456	2.3	155 571	2.1

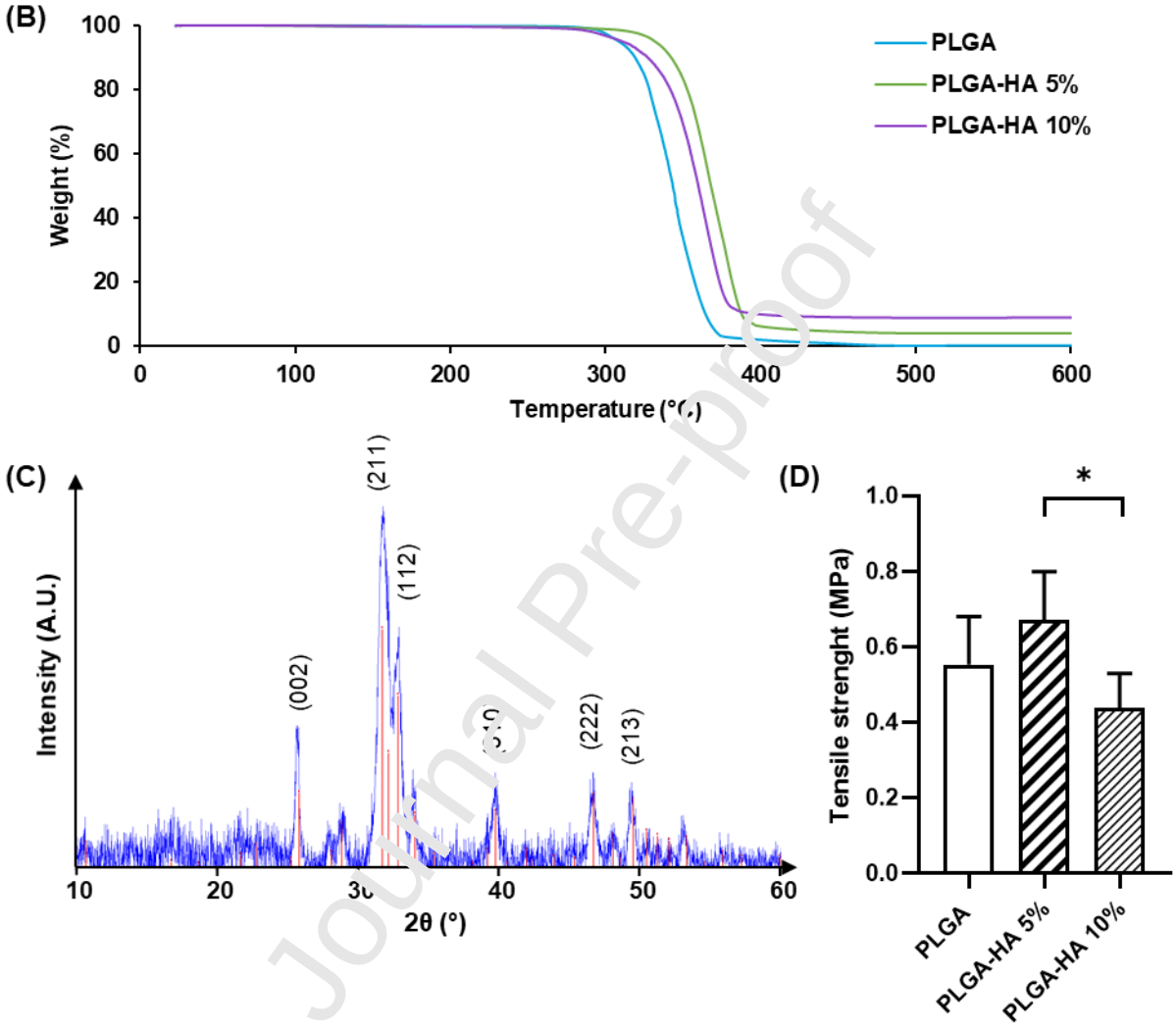

Figure 2. Physicochemical characterization of material. PLGA, PLGA-HA 5% and PLGA-HA 10% samples (before and after printing) were dissolved in THF and filtered. Mass average molecular weight ($\bar{M}_w$) and polydispersity index (PDI) were evaluated by SEC to show potential chemical degradation during manufacturing steps. Measurements in THF were performed on an Ultimate 3000 system (Thermoscientific) equipped with a diode array detector. Polystyrene was used as standard **(A)**. PLGA pellets (raw material) and materials before and after printing were analyzed by thermogravimetric analysis. The samples were warmed from 25°C to 900°C by 10°C/min then an isotherm was performed during 60min at 900°C **(B)**. The XRD patterns of PLGA-HA 10% scaffold was obtained with Cu-Kα beam conditions of 40 kV and 40 mA with collection of a spectrum at 2θ= 10°–60° and a step size of 0.1° **(C)**. An unaxial tensile test were conducted at 10 mm/min until failure to evaluate tensile strength. Data are mean ±SD (n=6, * $p<0.05$) **(D).**

of the $\bar{M}_w$ after shaping PLGA in a filament. But there was a difference between materials loaded or not with nHA. The printing process did not affect significantly $\bar{M}_w$ and PDI for the different loaded materials. However, a decrease of PDI was observed with PLGA after printing. TGA was used to control nHA loading

after shaping the materials in filaments (Fig. 2.B). The PLGA dissipation occurred on a short temperature range between 300°C and 400°C; the degradation was poorly impacted by the nHA dispersion. Nonetheless, the addition of nHA led to a slight increase of the temperature degradation of 21.6°C and 18.9°C with 5% and 10% of nHA respectively (Fig. 2.B). This effect tends to show that chemical bonds (at least Van Der Waals interactions) take place between the PLGA and the hydroxyapatite particle surfaces. Whatever, the temperature of PLGA material degradation was significantly higher than the printing temperature. TGA analysis revealed that nHA contents were 3.99% and 8.95% for PLGA-HA 5% and PLGA-HA 10% respectively, showing that the efficient weight concentration of nHA in PLGA was close to the target concentration. Fig. 2.C shows the XRD patterns of the PLGA-HA 10% printed material. Spectrums of PLGA and PLGA loaded with HA were distinct. No diffraction peaks were observed for the PLGA sample, showing the PLGA was amorphous, whereas characteristic peaks of nHA appeared for PLGA-HA 5% (data not shown) and PLGA-HA 10% (Fig. 2.C). nHA was identified, thanks to peak positions (cell parameters) and peak intensity ratios (relative to atomic content) as $Ca_9HPO_4(PO_4)_5OH$ (JCPDS 46-0905), a calcium deficient nHA, but with hydroxyapatite structure. Finally, mechanical properties of our material were evaluated with tensile tests (Fig.2.D). Addition of nHA did not lead to a statistical change of tensile strength compared to pure PLGA materials. PLGA-HA 10% scaffolds showed lower tensile strength compared to PLGA-HA 5%.

3.3. Nano-Hydroxyapatite distribution

MicroRaman spectroscopy was done on material with and without nHA, before (filaments) and after printing (scaffolds) to evaluate nHA distribution (Fig. 3.A/B). Spectra of material after printing (data not shown) were similar to spectra before printing (Fig. 3.A). Distinct profiles between material with and without nHA were obtained with MicroRaman spectroscopy (Fig. 3.A). Raman spectra of nHA showed characteristics peaks: A phosphate peak (PO_4^{3-}: 960cm^{-1}) and a hydroxide peak (OH: 3600cm^{-1}) (Fig. 3.A). The phosphate peak was used to map nHA distribution (Figure 3B). nHA was well distributed in PLGA-HA 5% and PLGA-HA 10% materials before and after printing. Spatial distribution of nHA was also observed after MicroCT imaging (Fig. 3.C). 3D reconstruction confirmed previous observations, nHA was well dispersed in PLGA-HA 5% or PLGA-HA 10% materials before and after printing (Fig. 3.C). Observations have shown that nHA particle size was heterogeneous inside the composite materials.

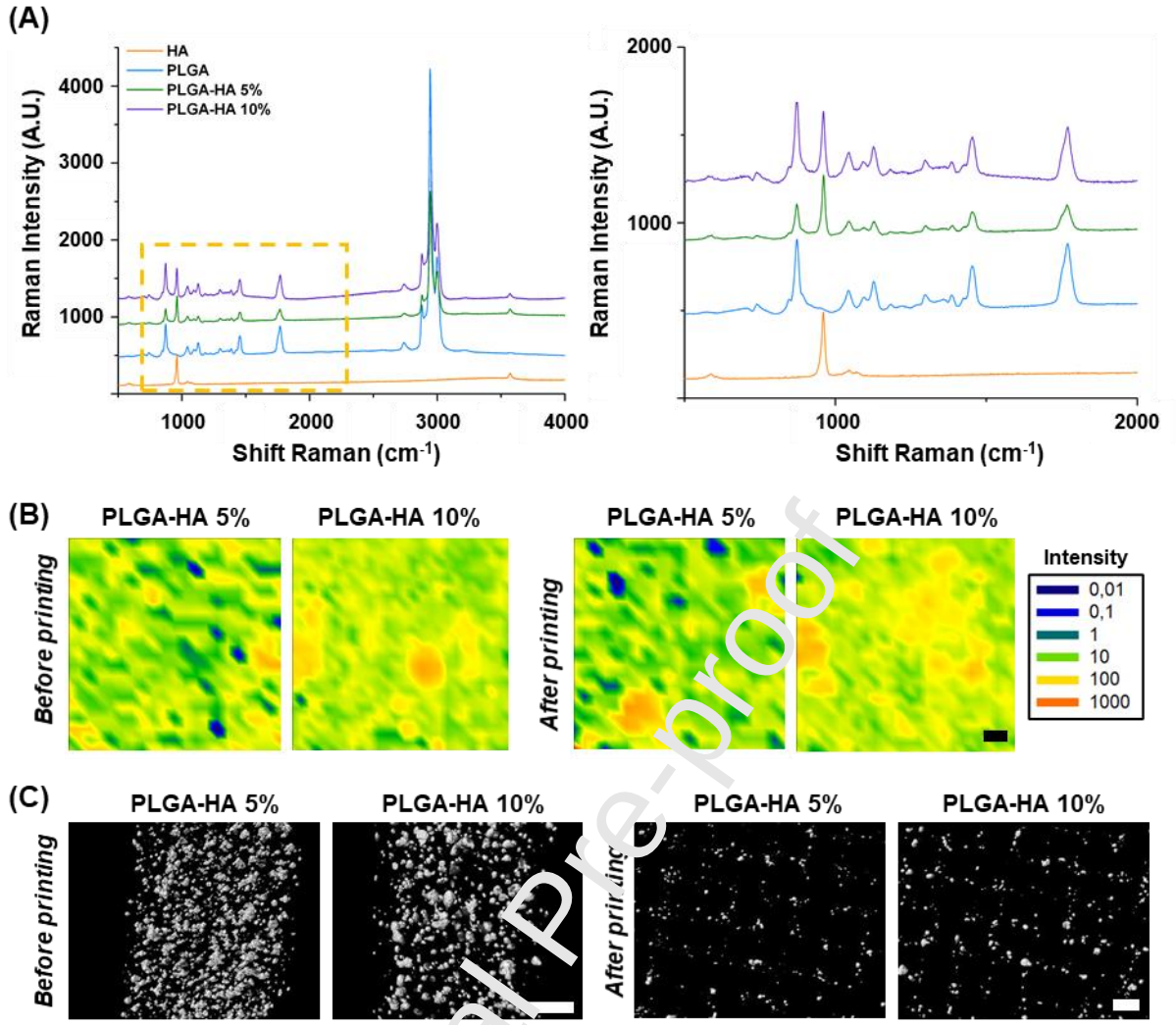

Figure 3. HA distribution before and after printing in HA charged materials. Spectrum of different printed materials was recorded by MicroRaman using a 532 nm laser for excitation. Graphic on the right correspond to the area delimited by yellow dotted line on left graphic. Spectra of HA showed characteristics peaks (PO_4^{3-} : 960 cm^{-1}; OH: 3600 cm^{-1}) **(A)**. Phosphate peak was used to show HA distribution in PLGA-HA 5% and PLGA-HA 10% before and after printing (Scale bar = 10 µm) **(B)**. PLGA-HA 5% and PLGA-HA 10% materials were scanned before and after printing by Micro-CT to observe spatial distribution of HA (Scale bar = 500 µm) **(C)**.

3.4. *In vitro* degradation of the materials

PLGA is known to be a biodegradable polymer, which releases acidic products during degradation. We studied its degradation *in vitro* for 15 weeks. After 10 weeks of degradation, PLGA and PLGA-HA 10% scaffolds became easily breakable during handling. The observation of the structure by SEM showed that

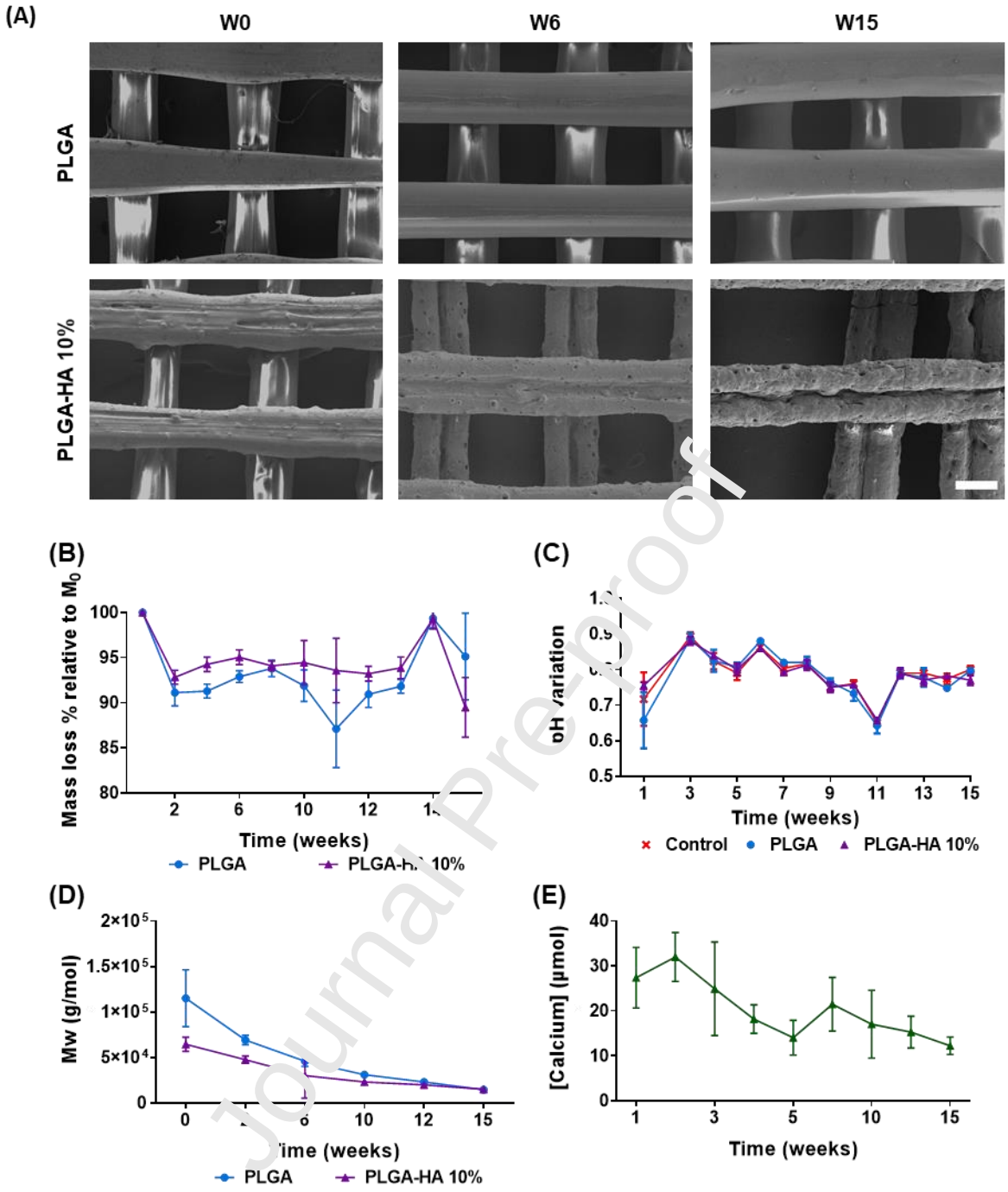

Figure 4. Degradation *in vitro*. According to the ASTM-F1635 norm, PLGA and PLGA-HA 10% scaffolds were immersed in PBS and incubated at 37°C in a 5% CO_2 incubator for 15 weeks. Membranes were observed by SEM, after Ni coating, to evaluate structural changes at weeks 0, 6, 15 (Scale bar = 200 µm) **(A)**. At different time points (2, 4, 6, 8, 10, 11, 12, 13, 14, 15 weeks) scaffolds were weighed and we defined week 0 as the baseline. Data are mean ±SD, n=4. **(B)**. Each week pH variation was measured with a pHmeter. Data are mean ±SD, n=4. **(C)**. Chemical degradation was evaluated by SEC (0, 2, 6, 10, 12, 15 weeks) to observe evolution of the mass average molecular weight ($\bar{M}_w$). Data are mean ±SD, n=3. **(D)**. The released Ca^{2+} was measured in collected PBS collected with a fluorometric assay kit. Data are mean ±SD, n=4. **(E)**.

PLGA scaffolds remained intact with a smooth surface, but they tended to twist (Fig. 4.A). PLGA-HA 10% scaffolds revealed an eroded surface and the threads appeared thinner every week (Fig. 4.A). A furrow appeared in the middle of the threads and small pores arose on the whole surface (Fig. 4.A). During the first

2 weeks, a weight loss of 8.9 ± 1.5 % and 7.2 ± 1.9 %, was observed for PLGA and PLGA-HA 10% materials, respectively (Fig. 4.B). During the following weeks, the mass remained stable, no significant mass loss was observed (Fig. 4.B). We assumed that observed degradation could be due to polymer chains degradation, the average molecular weight ($\bar{M}_w$) being a good indicator. $\bar{M}_w$ decreased for both materials throughout the experiment (Fig. 4.D). At the beginning, the $\bar{M}_w$ was $1.02x10^5 \pm 3.15x10^4$ g/mol, $6.45x10^4 \pm 7.83x10^3$ g/mol, for PLGA and PLGA-HA 10%, respectively (Fig. 4.D). After 15 weeks, the $\bar{M}_w$ was $1.46x10^4 \pm 2.94x10^3$ g/mol, $1.50x10^4 \pm 1.07x10^3$ g/mol, for PLGA and PLGA-HA 10%, respectively (Fig. 4.C). These observations revealed a chemical degradation of the materials. The pH remained stable during the entire experiment and it was similar to the control at each time point (Fig. 4.C). An important calcium release was observed during the first 3 weeks (Fig. 4.E). The average calcium release was 27.39 ± 6.74 µmol, 25.22 ± 5.44 µmol, 20.58 ± 10.40 µmol, for the week 1, 2 and 3 respectively (Fig. 4.E). From week 4 to 15, the average calcium release decreased. The average calcium release was 3.37 ± 1.94 µmol for the week 15 and it was significantly lower compared to week 1 (Fig. 4.E).

3.5. *In vitro* biocompatibility

We assessed the cytotoxicity of products released from scaffolds in cell culture medium over time (Fig. 5.A/B). The rinse extracts were prepared by soaking the scaffolds in media during 24h (E1), 48h (E2) and 72h (E3) (Fig. 5). Both cell types were in contact with rinse extracts of material during 24h. Cell viability and metabolic activity were not affected by media extracts of the printed scaffolds (Fig. 5.A/B). Both parameters remained significantly higher than 70% of the control.

According to ISO 10993-5, these results confirmed the absence of cytotoxic effect of the different materials evaluated. Then, we have examined the cell viability of both cell types onto printed scaffolds (Fig. 5.C). After 7, 14 and 21 days, both cell types were present on porous materials and a majority of living cells (green fluorescence) was observed, with only rare dead cells (red fluorescence). Cell proliferated on the scaffolds, especially hADSCs that appeared more numerous compared to hBMSCs, on both scaffolds. At day 14 hADSCs started to form a bridge-like structure and colonized the pores (Fig. 5.C).

3.1. *In vitro* cell differentiation

ALP is an early marker of osteoblastic differentiation. The first detected activity was around day 14 for both cell types (Fig. 6.A). The staining appeared more intense with PLGA-HA 10% scaffolds relative to PLGA for both cell types. Addition of osteoinductive media increased ALP activity of both cell types on PLGA and PLGA-HA 10% scaffolds.

Alizarin red reacts with calcium, thereby helping in the diagnosis of calcium deposits. We observed and quantified the staining after 21 days (Fig. 6.B/C). As control, cells were seeded on plastic wells and the amount of detected calcium was low. When cells were seeded on PLGA scaffolds, we observed that mineralization was similar to control. When cells were seeded on nHA-loaded scaffolds, the staining was stronger using both cell types. The use of osteoinductive media increased mineralization for both cell types. Using PLGA-HA 10% scaffolds led to a significantly higher calcium deposit by hADSCs compared to PLGA scaffolds. No significant difference was noted with hBMSCs seeded on the two different scaffolds.

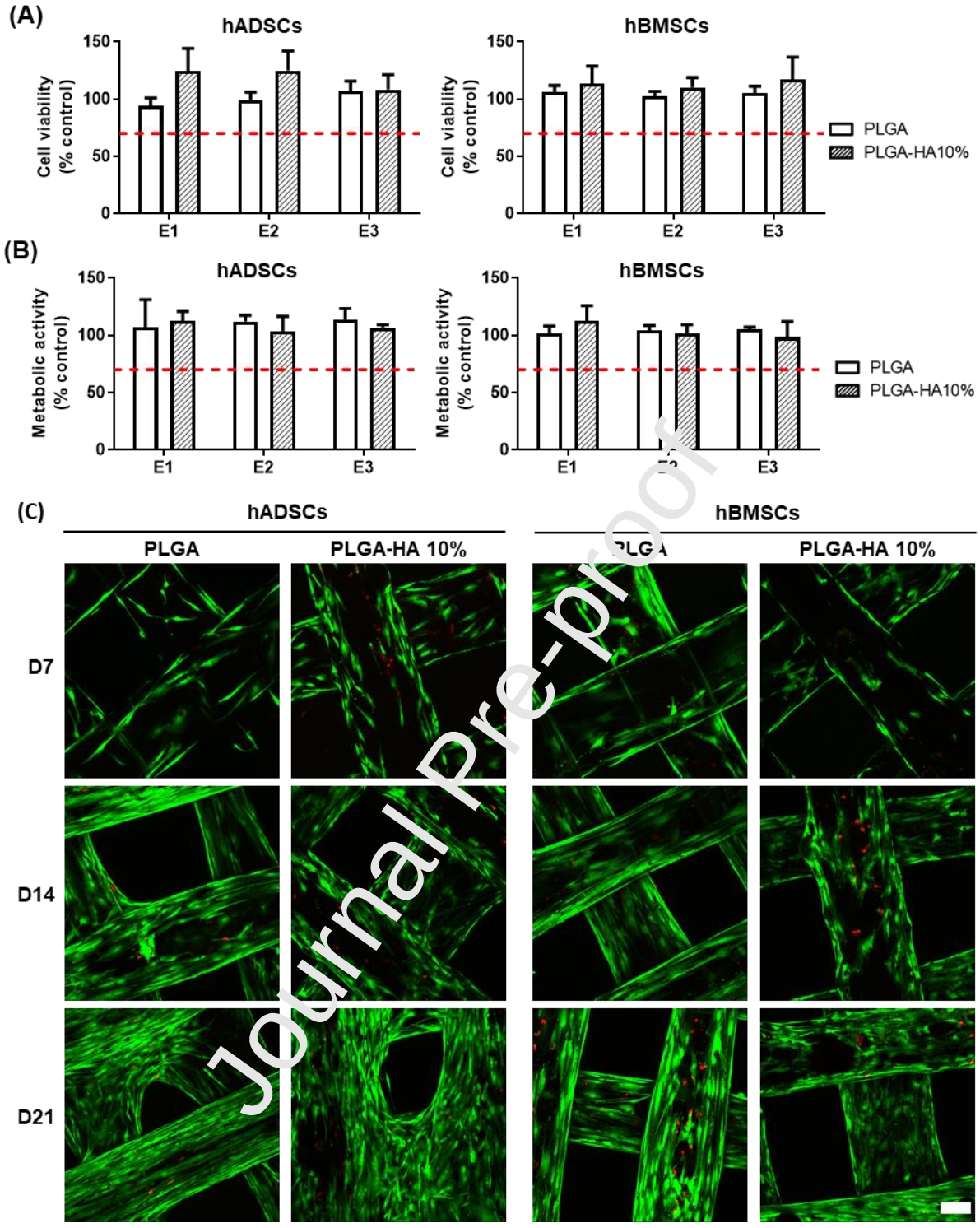

Figure 5. ***In vitro*** **evaluation of materials biocompatibility.** Potential cytotoxicity of materials toward hADSCs or hBMSC was evaluated using both MTT assay **(A)** and Neutral Red (NR) assay **(B)** and according to the NF-EN-ISO 10993-5 standard. Confluent cells were cultured during 24h with medium previously incubated during 24h (E1), 48h (E2), and 72h (E3) with scaffolds. Confluent cells cultured during 24h with regular medium or with 0.1% Triton 100X were used as negative and positive control, respectively. Results were expressed in percentage compared to the negative control. On each graph, the dotted line indicates the limit (70%) of cytotoxicity according to NF-EN-ISO 10993-5 standard. Data are mean ±SD, n=5. hADSCs and hBMSCs were seeded on PLGA and PLGA-HA 10% scaffolds and cell viability was evaluated after 7, 14 and 21 days of culture using fluorescent microscopy after live/dead staining (green/red) (n=3) (Scale bar = 100 µm) **(C)**.

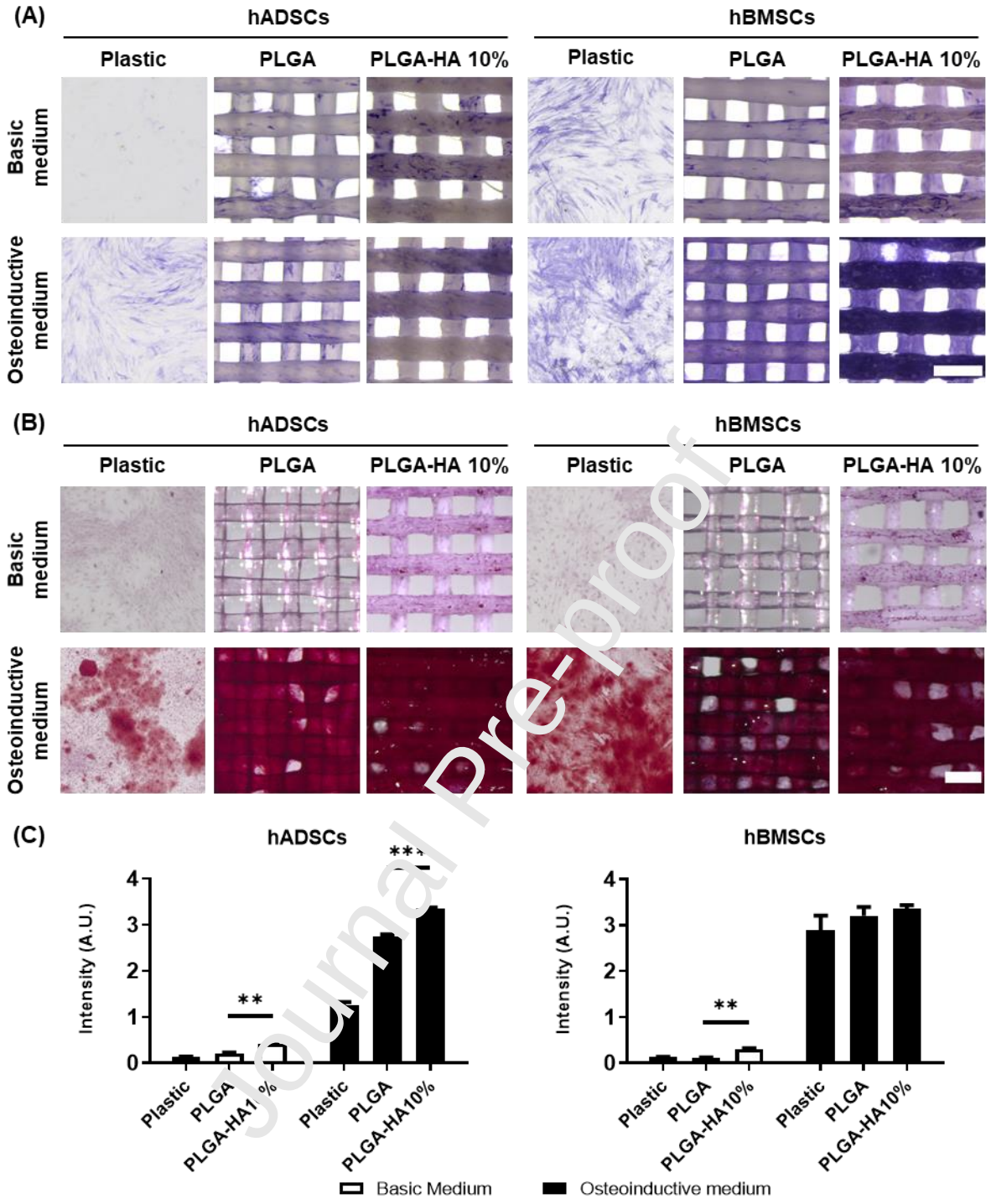

Figure 6. Evaluation of material osteodifferentiation potential. hADSCs and hBMSCs were seeded on PLGA, PLGA-HA 10% scaffolds or plastic well as control. After 14 days of culture, with or without osteoinductive media, ALP activity was evaluated by cells staining (Scale bar = 500 µm, n=3) **(A)**. After 21 days of cell culture, with or without osteoinductive media, mineralization was evaluated by Red Alizarin staining (Scale bar = 500 µm) **(B)**. The staining was extracted from materials and the supernatant was collected for absorbance measurements at 570 nm to quantify the mineralization. Data are mean ±SD (n=5, * $p<0.05$, ** $p < 0.01$, and *** $p < 0.001$) **(C)**.

3.2. *In vivo* biocompatibility

To evaluate the host response, a blinded independent trained investigator scored the inflammatory reaction around the implants semi quantitatively on histological sections stained with HES (Fig. **7.**A). Values were expressed as the difference between the test sample (PLGA and PLGA-HA 10% scaffolds) and the

sham-operated control (Fig. 7.B). One week after surgery a slight inflammatory reaction was observed around the different scaffolds. The size of fibrosis infiltrate was different, depending on the material: a moderately thick band was present around PLGA scaffolds but with PLGA-HA 10 %, a narrow band was present. An important cell infiltration was noticed. After 4 weeks, the fibrosis evolved to a thick band for PLGA scaffolds and to moderately thick for PLGA-HA 10% scaffolds. An important cell infiltration was still observed. Based on ISO 10993-6:2007 scoring, both materials were considered slightly irritant to the tissue when compared to the sham-operated control (Fig. 7).

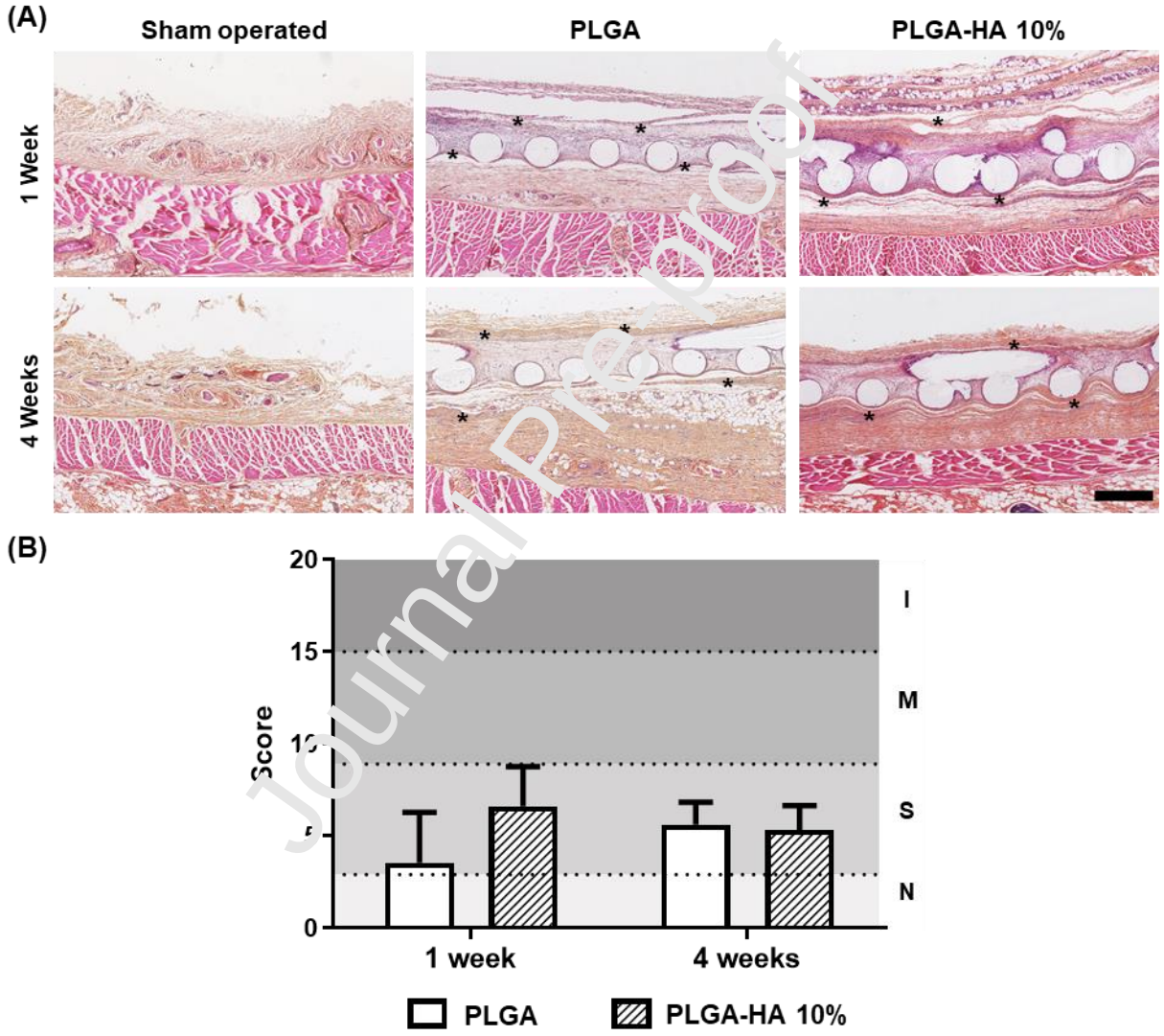

Figure 7. ***In vivo*** **biocompatibility.** PLGA and PLGA-HA 10% porous scaffolds were implanted subcutaneously in rats for 1 or 4 weeks. A sham-operated control was performed, with no biomaterial implantation. Histological sections were stained with HES for observation. A fibrosis band (indicated by *****) was observable around scaffold as a high cell infiltration (Scale bar = 500 µm) **(A)**. Histological sections were evaluated and scored according to NF-ENISO 10993-6 standard. The test samples were considered as non-irritant (N: up to 2.9), slightly (S: 3.0 up to 8.9) to moderately irritant (M: 9.0 up to 15.0) and severely irritant (I > 15) to tissue as compared to sham-operated control sample (n=8 samples per condition at one week, n=12 samples at 4 weeks) **(B)**.

4. Discussion

New methods for scaffold fabrication by additive manufacturing require a development of specific biomaterials. We selected PLGA for its medically-approved status and its limited degradation time, compared to other usual polymers [23]. PLGA presents a relatively low osteoconductive potential, but it was reported that the addition of HA could solve this issue [24]. For that reason, we have added HA nanoparticles to PLGA to improve its overall bioactivity for applications in bone tissue engineering. The osteoconductive properties of HA were demonstrated before in the literature [17]. To our knowledge, this composite biomaterial (PLGA + nHA) was never used before with FDM.

FDM is widely used in bone tissue engineering, because of its easy use and low cost. FDM enables creation of controlled and regular 3D-structure in a reproductive manner (Fig. 1) [7,25]. The molten polymer leaves the extruder in a liquid shape and should solidify immediately on the receiving platform to minimize the flow and maintain the expected printed pattern. We used a custom Fused Deposition Modeling 3D printer with high resolution, allowing to precisely control architecture of our scaffolds [19]. In this study, we observed that depending on the materials, dimensions of the printed structure could vary, in comparison with the initial files. PLGA-HA 10% composite biomaterial offered the most accurate final pattern compared to the other tested materials (Fig. 1). Indeed, the expansion of PLGA materials were lower and it led to an increased pore area in the final scaffold (Fig. 1). Nyberg et al. already observed a similar phenomenon when they compared the printing quality of PCL mixed with different minerals [26]. When PCL was mixed with HA, they obtained a more accurate final structure than PCL alone or PCL with other mineral dopants. This phenomenon could be explained by a variation of material viscosity, the difference of viscosity will impact material expansion on platform after printing.

Previous experiments have shown that a high ratio of mineral content could lead to a reduced printability of the materials [26,27]. Using FDM technique, a clogging of the printing head can occur when composite polymers loaded with high content of mineral are used [27]. Moreover, a higher printing temperature is usually required to print polymer-mineral composite materials with high percentage of mineral [26]. Regarding these observations, we chose a low nHA concentration in order to obtain a good printing quality and reproducibility. In our case, when nHA concentration was increased, the printing temperature was decreased. Damadzadeh et al. already observed a similar phenomenon with micro and nanoparticles of HA [15]. They demonstrated that an increased hydroxyapatite concentration led to a reduced

melting temperature of PLGA-HA composite [15] and this was probably due to a decreasing viscosity in presence of nHA. As the printing temperature of a polymer is directly linked to its melting temperature, the addition of calcium phosphates could be used to tune printing properties of composite materials.

Physicochemical properties of different components of our composite material were characterized before and after printing. First, chemical degradation of the polymer occurring during the different fabrication steps was evaluated by the molar mass changes. Three different printed materials (PLGA, PLGA-HA 5%, PLGA-HA 10%) were compared to the raw PLGA and filament materials (before printing) of the same type. $\bar{M}_w$ decreased after nHA addition (Fig. 2), this effect was already observed when minerals were added to a polymer [16,28]. It was hypothesized that the varying viscosity resulted in different shear stress during fabrication of the filament by extrusion. In our experiments, the printing process did not affect significantly the $\bar{M}_w$ of the materials. Previous reports have shown that the heating process always resulted in a decrease of molar mass [12]. Nevertheless, it was also noticed that the effect of heating on a polymer can differ from one material to another and it can vary depending on the polymer/mineral ratio [12]. TGA was used to compare real mineral charge to the expected one. Figure 2B reveals that the nHA loading was slightly lower than expected. It was observed elsewhere that the use of HA nanoparticles is more efficient than bigger particles to obtain expected mineral loading [15]. TGA can also be used to evaluate variation of materials degradation temperature, in order to assess their thermal stability. The addition of nHA helped to increase thermal stability by increasing degradation temperature (Fig. 2.B). This observation confirmed that the printing temperature, far below degradation temperature, should not lead to a degradation of the materials. Lastly, crystallographic analyses by XRD showed a pattern compatible with calcium-deficient HA. Natural bone is generally constituted of nanocrystalline, non-stoichiometric, calcium-deficient apatites [29]. Calcium-deficient hydroxyapatite showed higher dissolution and better bioactivity compared to stoechiometric HA [30,31]. Mechanical tests were performed to evaluate potential changes due to nHA presence. No significant changes were observed in tensile strength when nHA was added, compared to pure PLGA (Fig. 2.D). This result was expected considering the low nHA concentration used. However, PLGA-HA 10% scaffold showed a lower tensile strength than PLGA-HA 5%. The addition of mineral has been described to decrease mechanical properties depending on its concentration [15].

SEM images revealed a uniform distribution of the particles (likely nHA) along the surface of 3D-printed threads (Fig. 1.B). The presence of nHA on the surface is crucial to increase cell contact and cell signaling, in order to improve cell adhesion, proliferation and osteodifferentiation. nHA distribution was evaluated by Raman microscopy and Micro-CT. Both techniques showed a homogenous distribution of nHA inside the composite materials before and after printing (Fig. 3.B/C). Micro-CT observations showed that nHA was homogenously distributed in the entire filaments and printed scaffolds (Fig. 3.C). The presence of nHA inside the materials threads may be advantageous for long-term accessibility of the particles, as they will be more exposed when the PLGA degrades. Observations of nHA distribution also showed that particle size was different inside materials before and after printing (Fig. 1). The nHA particles might clump during the filament fabrication process.

One of the qualities expected for a material applied in bone tissue engineering is the biodegradability. The material resorption should follow bone regeneration. First place, the material should be a support for bone ingrowth. Then, the material should be degraded, before it is replaced by newly-formed bone [32]. During first weeks of *in vitro* degradation, the morphology of the scaffolds remained stable. However, slight changes of PLGA-HA 10% began after 6 weeks of incubation in PBS: the scaffolds revealed an eroded surface, a furrow appeared in the middle of the threads as well as small pores (Fig. 4.A). These changes were more visible every week. After 10 weeks, the texture of PLGA and PLGA-HA 10% scaffolds began to become more fragile. Moreover, PLGA scaffolds started to deform. Liu et al. observed the same phenomenon with PLGA scaffolds after 10 weeks [33]. After 15 weeks, the mass loss was limited for the different scaffolds, inferior to 15% of the initial mass. One study showed a relative limited mass loss of PLGA scaffolds, even after 10 weeks of *in vitro* degradation following similar protocol [33]. It was observed elsewhere that the mass loss occurred if molecular chains were reduced to a size that allowed their free diffusion out of the polymer matrix [34,35]. Usually, PLGA-like polymers undergo bulk degradation [36,37]. Molecular weight of a polymer is rapidly affected upon placement in an aqueous media [38]. This is exactly what we observed during the degradation of both scaffold types: the degradation was fast during the first 6 weeks and then it slowed down (Fig. 4.D). During *in vitro* degradation, the pH was not affected by degradation of PLGA or PLGA-HA 10% (Fig. 4.C). PLGA degradation is generally followed by a release of acidic by-products, as described Hasirci et al. [37]. *In vivo*, release of acidic products could result in

important inflammatory reactions, which was not observed in our study. It is known that HA produce basic products during resorption [39–41] and in our case, it might have buffered the acidic products of PLGA; thereby, it may help to reduce the formation of an acidic environment that would be deleterious for surrounding tissues [39–41]. Regarding HA, we observed different phases of calcium release (Fig. 4.E). An important calcium release was observed during the first 3 weeks, followed by a decrease of the release from week 4 to 15. These variations in calcium release could be explained by the different phases of PLGA degradation. First, a surface erosion was observed, leading to the formation of pores observed by SEM (Fig. 4.A), probably related to nHA particles release. Then, the rate of calcium release slowed down because PLGA degradation was limited and did not leave access to inner nHA particles.

An ideal biomaterial should provide a biocompatible structural support for cells, which must adhere and proliferate. Biocompatibility of the composite materials was also evaluated *in vitro* using two cell types: hBMSCs and hADSCs. These cells were chosen because of their relevance in bone tissue engineering applications as they have already been used in clinics [42]. According to the NF EN 30993-5 ISO 10993-5 both materials revealed no cytotoxic effects (Fig. 5.A/B). A good cell viability as well as stable metabolic activity were observed. Moreover, high cell colonization and cell viability were observed on both scaffolds from the first to the third week of cell culture (Fig. 5.C). No differences of cell colonization were observed between the materials, showing that nHA did not impair cell colonization.

PLGA degradation products are described as non-toxic, but the release of acidic products, such as lactate, can induce local inflammation. We assessed the inflammation potential of our materials using subcutaneous implantation in rats. After 4 weeks, materials were not resorbed (Fig. 7.A). We observed that PLGA and PLGA-HA 10% induced a slight inflammatory reaction as compared to the sham-operated control samples (Fig. 7.B). *In vitro* degradation results showed that pH was not affected, even after 15 weeks, which could explain the relatively slight reaction. The *in vivo* study showed important cell infiltration, probably macrophages, after 1 week (Fig. 7.A). This infiltration was still observable after 4 weeks (Fig. 7.A). Xia et al. also demonstrated that macrophages actively responded to PLGA materials and degrade the surface of the materials [43]. PLGA is described as a biodegradable polymer in literature, making it useful in many short-term medical applications. These observations led us to conclude that the composite materials were

biocompatible and induced their own biodegradation. PLGA, HA and their combinations have already been proven as biocompatible [41,44].

Several studies have shown the added value of minerals incorporation into a polymer matrix [10,12] for bone tissue engineering applications, because this generally promotes development of an osteoblastic phenotype of the implanted cells [10,12]. In the presence of nHA, the ALP activity was higher and the production of mineralized matrix was significantly increased (Fig. 6). The first detected ALP activity was late, around day 14 for both cell types (Fig. 6A). The ALP activity appeared higher with PLGA-HA 10% materials relative to PLGA for both cell types and it increased over time. Regarding mineral deposition, we observed that mineralization on PLGA was similar as with cells seeded on plastic (Fig. 6.B/C). Interestingly, when cells were seeded on nHA-loaded materials, mineralization was higher using both cell types. With osteoinductive media (positive controls), the calcium deposition was significantly increased as well. With hADSCs we observed a potentiated effect with PLGA-HA 10% using osteoinductive media. Finally, it appeared that the amount of nHA used in the study was sufficient to enhance osteoblastic differentiation and matrix mineralization. In this study, the presence of nHA seemed to offer favorable characteristics for bone tissue engineering applications.

5. Conclusion

In this study, we have developed a PLGA-HA composite material for the fabrication by FDM of 3D scaffolds for bone tissue engineering. These composite biomaterials were printable with good reproducibility. Our manufacturing process did not induce significant chemical degradation of the materials and the nHA loading was maintained. The nHA distribution was homogeneous on the surface as well as inside the material threads. The biocompatibility was broadly confirmed through *in vitro* and *in vivo* experiments, and *in vitro* results revealed osteopromotive potential of this composite material. To conclude, our data demonstrate that we developed a biomaterial with favorable properties and relevant cellular response for bone tissue engineering applications.

6. Acknowledgements

The authors would like to thank Emmanuel Pauthe, Michel Boissière, Sylvain Bourrasseau and Amélie Vax for their technical help and support. We are thankful for the access to Micro-CT by IHU-Lyric

and for the precious advices of Richard Walton. SEM micrographs were realized at Microscopies & Analyses core facility (CY Cergy Paris Université) supported by Région Ile de France through the SESAME project. All Raman experiments have been performed at the platform SIV at University of Bordeaux, funded by the FEDER and the Region Aquitaine. This work was supported by the Agence Nationale de la Recherche (ANR-16-CE18-0009-01).

References

[1] A. Wubneh, E.K. Tsekoura, C. Ayranci, H. Uludağ, Current state of fabrication technologies and materials for bone tissue engineering, Acta Biomater. 80 (2018) 1–30. https://doi.org/10.1016/j.actbio.2018.09.031.

[2] M. Wang, C. Laurencin, X. Yu, Encyclopedia of Biomedical Engineering, Elsevier, 2018.

[3] A. D'Agostino, L. Trevisiol, V. Favero, M. Gunson, F. Bedica, P.F. Nocini, G.W. Arnett, Hydroxyapatite/Collagen Composite Is a Reliable Material for Malar Augmentation - ScienceDirect, J Oral Maxillofac Surg. 74 (2016) 1238.e1-1238.e15.

[4] G. Staffa, A. Barbanera, A. Faiola, M. Fricia, P. Limoni, R. Mottaran, B. Zanotti, R. Stefini, Custom made bioceramic implants in complex and large cranial reconstruction: A two-year follow-up, J. Cranio-Maxillofac. Surg. 40 (2012) e65–e70. https://doi.org/10.1016/j.jcms.2011.04.014.

[5] J.P. Temple, D.L. Hutton, B.P. Hung, P.Y. Huri, C.A. Cook, R. Kondragunta, X. Jia, W.L. Grayson, Engineering anatomically shaped vascularized bone grafts with hASCs and 3D-printed PCL scaffolds, J. Biomed. Mater. Res. A. 102 (2014) 4317–4325. https://doi.org/10.1002/jbm.a.35107.

[6] L. Moroni, T. Boland, J.A. Burdick, C. De Maria, B. Derby, G. Forgacs, J. Groll, Q. Li, J. Malda, V.A. Mironov, C. Mota, M. Nakamura, W. Shu, S. Takeuchi, T.B.F. Woodfield, T. Xu, J.J. Yoo, G. Vozzi, Biofabrication: A Guide to Technology and Terminology, Trends Biotechnol. 36 (2018) 384–402. https://doi.org/10.1016/j.tibtech.2017.10.015.

[7] I. Zein, D.W. Hutmacher, K.C. Tan, S.H. Teoh, Fused deposition modeling of novel scaffold architectures for tissue engineering applications, Biomaterials. 23 (2002) 1169–1185. https://doi.org/10.1016/S0142-9612(01)00232-0.

[8] S.J. Kalita, S. Bose, H.L. Hosick, A. Bandyopadhyay, Development of controlled porosity polymer-ceramic composite scaffolds via fused deposition modeling, Mater. Sci. Eng. C. 23 (2003) 611–620. https://doi.org/10.1016/S0928-4931(03)00052-3.

[9] L. Roseti, V. Parisi, M. Petretta, C. Cavallo, G. Desando, I. Bartolotti, B. Grigolo, Scaffolds for Bone Tissue Engineering: State of the art and new perspectives, Mater. Sci. Eng. C. 78 (2017) 1246–1262. https://doi.org/10.1016/j.msec.2017.05.017.

[10] B. Lei, B. Guo, K.J. Rambhia, P.X. Ma, Hybrid Polymer Biomaterials for Bone Tissue Regeneration, Front. Med. 13 (2019) 189–201. https://doi.org/10.1007/s11684-018-0664-6.

[11] C. Wang, W. Huang, Y. Zhou, L. He, Z. He, Z. Chen, X. He, S. Tian, J. Liao, B. Lu, Y. Wei, M. Wang, 3D printing of bone tissue engineering scaffolds, Bioact. Mater. 5 (2020) 82–91. https://doi.org/10.1016/j.bioactmat.2020.01.004.

[12] J. Babilotte, V. Guduric, D.L. Nihouannen, A. Naveau, J.-C. Fricain, S. Catros, 3D printed polymer–mineral composite biomaterials for bone tissue engineering: Fabrication and characterization, J. Biomed. Mater. Res. B Appl. Biomater. 107 (2019) 2579–2595. https://doi.org/10.1002/jbm.b.34348.

[13] F.S. Senatov, K.V. Niaza, M.Yu. Zadorozhnyy, A.V. Maksimkin, S.D. Kaloshkin, Y.Z. Estrin, Mechanical properties and shape memory effect of 3D-printed PLA-based porous scaffolds, J. Mech. Behav. Biomed. Mater. 57 (2016) 139–148. https://doi.org/10.1016/j.jmbbm.2015.11.036.

[14] N. Xu, X. Ye, D. Wei, J. Zhong, Y. Chen, G. Xu, D. He, 3D Artificial Bones for Bone Repair Prepared by Computed Tomography-Guided Fused Deposition Modeling for Bone Repair, ACS Appl. Mater. Interfaces. 6 (2014) 14952–14963. https://doi.org/10.1021/am502716t.

[15] B. Damadzadeh, H. Jabari, M. Skrifvars, K. Airola, N. Moritz, P.K. Vallittu, Effect of ceramic filler content on the mechanical and thermal behaviour of poly-lactic-co-glycolic acid composites for medical applications, J. Mater. Sci. Mater. Med. 21 (2010) 2523–2531. https://doi.org/10.1007/s10856-010-4110-9.

[16] R.L. Simpson, S.N. Nazhat, J.J. Blaker, A. Bismarck, R. Hill, A.R. Boccaccini, U.N. Hansen, A.A. Amis, A comparative study of the effects of different bioactive fillers in PLGA matrix composites and their suitability as bone substitute materials: A thermo-mechanical and in vitro investigation, J. Mech. Behav. Biomed. Mater. 50 (2015) 277–289. https://doi.org/10.1016/j.jmbbm.2015.06.008.
[17] S.V. Dorozhkin, Bioceramics of calcium orthophosphates, Biomaterials. 31 (2010) 1465–1485. https://doi.org/10.1016/j.biomaterials.2009.11.050.
[18] A. Afshar, M. Ghorbani, N. Ehsani, M.R. Saeri, C.C. Sorrell, Some important factors in the wet precipitation process of hydroxyapatite, Mater. Des. 24 (2003) 197–202. https://doi.org/10.1016/S0261-3069(03)00003-7.
[19] A. Grémare, V. Guduric, R. Bareille, V. Heroguez, S. Latour, N. L'heureux, J.-C. Fricain, S. Catros, D.L. Nihouannen, Characterization of printed PLA scaffolds for bone tissue engineering, J. Biomed. Mater. Res. A. 106 (2018) 887–894. https://doi.org/10.1002/jbm.a.36289.
[20] J.M. Seong, B.-C. Kim, J.-H. Park, I.K. Kwon, A. Mantalaris, Y.-S. Hwang, Stem cells in bone tissue engineering, Biomed. Mater. Bristol Engl. 5 (2010) 062001. https://doi.org/10.1088/1748-6041/5/6/062001.
[21] J. Vilamitjana-Amedee, R. Bareille, F. Rouais, A.I. Caplan, M.F. Harmand, Human bone marrow stromal cells express an osteoblastic phenotype in culture, In Vitro Cell. Dev. Biol. Anim. 29A (1993) 699–707.
[22] F. Villars, B. Guillotin, T. Amédée, S. Dutoya, L. Bordenave, R. Bareille, J. Amédée, Effect of HUVEC on human osteoprogenitor cell differentiation needs heterotypic gap junction communication, Am. J. Physiol.-Cell Physiol. 282 (2002) C775–C785. https://doi.org/10.1152/ajpcell.00310.2001.
[23] B.S. Kim, J. Jang, S. Chae, G. Gao, J.-S. Kong, M. Ahn, D.-W. Cho, Three-dimensional bioprinting of cell-laden constructs with polycaprolactone protective layers for using various thermoplastic polymers, Biofabrication. 8 (2016). https://doi.org/10.1088/1758-5090/8/3/035013.
[24] P. Gentile, V. Chiono, I. Carmagnola, P.V. Hatton, An Overview of Poly(lactic-co-glycolic) Acid (PLGA)-Based Biomaterials for Bone Tissue Engineering, Int. J. Mol. Sci. 15 (2014) 3640–3659. https://doi.org/10.3390/ijms15033640.
[25] T. Serra, M. Ortiz-Hernandez, E. Engel, J.A. Planell, M. Navarro, Relevance of PEG in PLA-based blends for tissue engineering 3D-printed scaffolds, Mater. Sci. Eng. C. 38 (2014) 55–62. https://doi.org/10.1016/j.msec.2014.01.003.
[26] E. Nyberg, A. Rindone, A. Dorafshar, W.L. Grayson, Comparison of 3D-Printed Poly-ε-Caprolactone Scaffolds Functionalized with Tricalcium Phosphate, Hydroxyapatite, Bio-Oss, or Decellularized Bone Matrix, Tissue Eng. Part A. 23 (2017) 503–514. https://doi.org/10.1089/ten.tea.2016.0418.
[27] B.P. Hung, B.A. Naved, E.L. Nyberg, M. Dias, C.A. Holmes, J.H. Elisseeff, A.H. Dorafshar, W.L. Grayson, Three-Dimensional Printing of Bone Extracellular Matrix for Craniofacial Regeneration, ACS Biomater. Sci. Eng. 2 (2016) 1806–1816. https://doi.org/10.1021/acsbiomaterials.6b00101.
[28] J. Idaszek, A. Bruinink, W. Święszkowski, Ternary composite scaffolds with tailorable degradation rate and highly improved colonization by human bone marrow stromal cells, J. Biomed. Mater. Res. A. 103 (2015) 2394–2405. https://doi.org/10.1002/jbm.a.35377.
[29] C. Drouet, Apatite Formation: Why It May Not Work as Planned, and How to Conclusively Identify Apatite Compounds, BioMed Res. Int. 2013 (2013) e490946. https://doi.org/10.1155/2013/490946.
[30] H. Li, M. Gong, A. Yang, J. Ma, X. Li, Y. Yan, Degradable biocomposite of nano calcium-deficient hydroxyapatite-multi(amino acid) copolymer, Int. J. Nanomedicine. 7 (2012) 1287–1295. https://doi.org/10.2147/IJN.S28978.
[31] J.H.C. Lin, K.H. Kuo, S.J. Ding, C.P. Ju, Surface reaction of stoichiometric and calcium-deficient hydroxyapatite in simulated body fluid, J. Mater. Sci. Mater. Med. 12 (2001) 731–741. https://doi.org/10.1023/A:1011280828663.
[32] C. Zizelmann, R. Schoen, M.C. Metzger, R. Schmelzeisen, A. Schramm, B. Dott, K.-H. Bormann, N.C. Gellrich, Bone formation after sinus augmentation with engineered bone, Clin. Oral Implants Res. 18 (2007) 69–73. https://doi.org/10.1111/j.1600-0501.2006.01295.x.
[33] C.-G. Liu, Y.-T. Zeng, R.K. Kankala, S.-S. Zhang, A.-Z. Chen, S.-B. Wang, Characterization and Preliminary Biological Evaluation of 3D-Printed Porous Scaffolds for Engineering Bone Tissues, Materials. 11 (2018). https://doi.org/10.3390/ma11101832.
[34] R.L. Kronenthal, Biodegradable Polymers in Medicine and Surgery, in: R.L. Kronenthal, Z. Oser, E. Martin (Eds.), Polym. Med. Surg., Springer US, Boston, MA, 1975: pp. 119–137. https://doi.org/10.1007/978-1-4684-7744-3_9.

[35] S.M. Li, H. Garreau, M. Vert, Structure-property relationships in the case of the degradation of massive poly(α-hydroxy acids) in aqueous media, J. Mater. Sci. Mater. Med. 1 (1990) 131–139. https://doi.org/10.1007/BF00700872.

[36] L.S. Nair, C.T. Laurencin, Biodegradable polymers as biomaterials, Prog. Polym. Sci. 32 (2007) 762–798. https://doi.org/10.1016/j.progpolymsci.2007.05.017.

[37] V. Hasırcı, K. Lewandrowski, J.D. Gresser, D.L. Wise, D.J. Trantolo, Versatility of biodegradable biopolymers: degradability and an in vivo application, J. Biotechnol. 86 (2001) 135–150. https://doi.org/10.1016/S0168-1656(00)00409-0.

[38] W.H. Wong, D.J. Mooney, Synthesis and Properties of Biodegradable Polymers Used as Synthetic Matrices for Tissue Engineering, in: A. Atala, D.J. Mooney (Eds.), Synth. Biodegrad. Polym. Scaffolds, 1997: pp. 51–82. https://doi.org/10.1007/978-1-4612-4154-6_4.

[39] C.M. Agrawal, K.A. Athanasiou, Technique to control pH in vicinity of biodegrading PLA-PGA implants, J. Biomed. Mater. Res. 38 (1997) 105–114. https://doi.org/10.1002/(sici)1097-4636(199722)38:2<105::aid-jbm4>3.0.co;2-u.

[40] A. Tiwari, A. Tiwari, Bioengineered Nanomaterials, CRC Press, 2013.

[41] N. Zhang, H.L. Nichols, S. Tylor, X. Wen, Fabrication of nanocrystalline hydroxyapatite doped degradable composite hollow fiber for guided and biomimetic bone tissue engineering, Mater. Sci. Eng. C. 27 (2007) 599–606. https://doi.org/10.1016/j.msec.2006.05.024.

[42] C. Colnot, Cell Sources for Bone Tissue Engineering: Insights from Basic Science, Tissue Eng. Part B Rev. 17 (2011) 449–457. https://doi.org/10.1089/ten.teb.2011.0243.

[43] Z. Xia, Y. Huang, I.E. Adamopoulos, A. Walpole, J.T. Triffitt, Z. Cui, Macrophage-mediated biodegradation of poly(DL-lactide-co-glycolide) in vitro, J. Biomed. Mater. Res. A. 79A (2006) 582–590. https://doi.org/10.1002/jbm.a.30853.

[44] S.-S. Kim, M. Sun Park, O. Jeon, C. Yong Choi, B.-S. Kim, Poly(lactide-co-glycolide)/hydroxyapatite composite scaffolds for bone tissue engineering, Biomaterials. 27 (2006) 1399–1409. https://doi.org/10.1016/j.biomaterials.2005.08.016.

Declaration of competing interests

☒ The authors declare that they have no known competing financial interests or personal relationships that could have appeared to influence the work reported in this paper.

☐The authors declare the following financial interests/personal relationships which may be considered as potential competing interests:

Author statement

Joanna Babilotte : Conceptualization, Methodology, Validation, Formal analysis, Investigation, Writing – Original Draft, Writing – Review & Editing, Visualization **Benoit Martin**: Validation, Formal analysis, Investigation **Vera Guduric:** Conceptualization, Formal analysis, Writing – Review & Editing **Reine Bareille:** Validation, Formal analysis, Investigation, Writing – Review & Editing **Rémy Agniel:** Validation, Formal analysis, Investigation **Samantha Roques:** Validation, Investigation **Valérie Héroguez:** Validation, Formal analysis, Investigation, Writing – Review & Editing **Marc Dussauze:** Validation, Formal analysis, Investigation, Writing – Review & Editing **Manuel Gaudon:** Validation, Formal analysis, Investigation, Writing – Review & Editing **Damien Le Nihouannen:** Conceptualization, Writing – Review & Editing, Supervision **Sylvain Catros:** Conceptualization, Writing – Review & Editing, Supervision, Project administration, Funding acquisition

Highlights

- Manufacturing steps have a minor impact on materials properties
- Materials provide a biocompatible and osteopromotive support over two cell type
- No major signals of inflammation observed, outlining material biocompatibility